A Dynamic Window-Based UWB-Odometer Fusion Approach for Indoor Positioning

Hui Zhang, *Member, IEEE*, Xidong Zhou, *Graduate Student Member, IEEE*, Hang Zhong, *Member, IEEE*, He Xie, Wei He, Xuan Tan, and Yaonan Wang

***Abstract*—The positioning system based on ultrawideband (UWB) can achieve centimeter-level positioning accuracy, which is now widely used for indoor positioning. However, UWB is subject to multipath effects and nonline-of-sight (NLOS), which can cause positioning errors. And a UWB positioning system with a minimum of three anchors is costly and difficult to deploy, which is not an economical option. This article presents a low-cost UWB-odometer fusion method for mobile robot localization, which enables global localization using only one UWB anchor. To improve the positioning accuracy and eliminate the influence of cumulative odometer error, we propose a dynamic window-based particle filter (DWBPF). It solves the problem of particle convergence and track loss. It also adaptively modifies the score weights according to the power difference of the UWB to achieve a more robust and accurate positioning. The experimental result shows that the system has a high positioning accuracy of 0.061 m.**

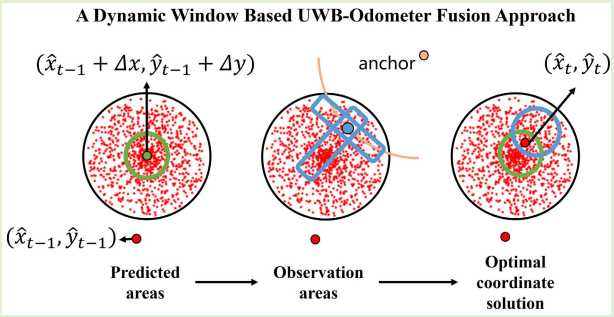

***Index Terms*—Indoor positioning, mobile robot, particle filter (PF), ultrawideband (UWB).**

I. Introduction

IN RECENT years, the application of mobile robots [1] has developed rapidly, such as meal delivery robots [2], inspection robots [3], and sweeping robots [4]. These mobile robots need to realize the fixed-point navigation function, so the positioning system plays an important role in these applications. While high-precision and stable positioning can be achieved outdoors using the global positioning system (GPS) [5], it is still a challenging task to achieve high-precision positioning indoors. Li et al. [6] pointed out that current stable and mature mobile robot positioning algorithms mainly include: Markov localization, particle filter (PF)-based approach, Rao-blackwellization filter-based approach, and matching technique based on laser scanning. Among them, the Monte Carlo localization based on probability graph [7] is now widely used. Batistić and Tomic [8] pointed out that current stable and mature indoor positioning system (IPS) technologies mainly include: wireless local area network (LAN), radio-frequency (RF) identification, ultrasonic, Bluetooth, odometry, and ultrawideband (UWB). These techniques mainly use fingerprinting, triangulation, and dead reckoning for position estimation. Among these technologies, odometry and UWB have the highest positioning accuracy.

The odometry includes wheel odometry, inertial odometry, laser odometry, radar odometry, and visual odometry. Wheel odometry has been used for many skid-steering robots, such as two- and four-wheel robots [9]. It is a simple and inexpensive localization technique for mobile robots. The wheel odometer uses an encoder to calculate each wheel's forward distance, and the mobile robot's displacement distance in the x-axis and y-axis directions is calculated through the kinematic model [10]. However, the Moiré fringe photoelectric signal subdivision error [11] in the encoder leads to errors in

Manuscript received 6 September 2022; revised 22 November 2022; accepted 10 December 2022. Date of publication 16 December 2022; date of current version 31 January 2023. This work was supported in part by the National Key Research and Development Program of China under Grant 2021ZD0114503; in part by the Major Research Plan of the National Natural Science Foundation of China under Grant 92148204; in part by the National Natural Science Foundation of China under Grant 62027810, Grant 61971071, and Grant 62133005; in part by the Hunan Leading Talent of Technological Innovation under Grant 2022RC3063; in part by the Hunan Science Fund for Distinguished Young Scholars under Grant 2021JJ10025; in part by the Hunan Key Research and Development Program under Grant 2021GK4011 and Grant 2022GK2011; in part by the Changsha Science and Technology Major Project under Grant kh2003026; in part by the Joint Open Foundation of State Key Laboratory of Robotics under Grant 2021-KF-22-17; and in part by the China University Industry-University-Research Innovation Fund under Grant 2020HYA06006. The associate editor coordinating the review of this article and approving it for publication was Dr. Qammer H. Abbasi. *(Corresponding author: Hui Zhang.)*

Hui Zhang is with the National Engineering Research Center of Robot Visual Perception and Control Technology, College of Robotics, Hunan University, Changsha, Hunan 410082, China (e-mail: zhanghuihby@126.com).

Xidong Zhou and Xuan Tan are with the College of Electrical and Information Engineering, Changsha University of Science and Technology, Changsha, Hunan 410000, China.

Hang Zhong, He Xie, and Yaonan Wang are with the National Engineering Research Center of Robot Visual Perception and Control Technology, College of Electrical and Information Engineering, Hunan University, Changsha, Hunan 410082, China.

Wei He is with the School of Intelligence Science and Technology, University of Science and Technology Beijing, Beijing 100083, China, and also with the Institute of Artificial Intelligence, University of Science and Technology Beijing, Beijing 100083, China.

Digital Object Identifier 10.1109/JSEN.2022.3228789

the displacement distance and causes uncorrectable odometry accumulation errors through constant motion, which cannot provide long time tracking. Despite all this, odometers are high-precision at tracking over short periods.

UWB-based IPS have no cumulative error in positioning but are affected by multipath effect, non-line-of-sight (NLOS), and other factors. In general, the uncertainty and spurious measurements during UWB ranging can be represented by an error model that combines a Gaussian distribution (for line-of-sight (LOS) measurements), a Gamma distribution (for NLOS measurements), and a constant value [12]. As for the errors caused by NLOS, they are currently reduced by two main methods: NLOS identification and NLOS mitigation. NLOS identification [13], [14] can be realized by checking the characteristics of the received signal or the statistics of a channel impulse response. And NLOS mitigation can be achieved through constrain optimization [15], maximum likelihood-based technique [16], and robust estimator [17]. Although NLOS introduces errors into the UWB positioning system, the long-term positioning accuracy of UWB-based positioning systems is still the highest in IPS technologies.

In order to improve localization accuracy, multisensor fusion algorithms are usually required to combine the advantages of each sensor, such as the Kalman filter (KF), Extended KF (EKF), or PF. PF has been widely used in localization systems and has shown good performance. The main challenges in applying PF to practical problems are properly modeling the system functions and noise distribution, real-time performance, and lost track issue [18]. As the effective number of particles decreases over time, the performance of the PF will also be affected. In dynamic positioning systems, certain conditions can lead to stranded particle clouds. For example, when the target velocity changes unexpectedly or when the environment forces a change in the trajectory, the particle cloud may be trapped indefinitely in the low probability region.

In this article, a dynamic window-based PF (DWBPF) method is proposed, which combines the idea of the dynamic window method (DWA) [19]. According to the equation of the robot's motion and the measured quality of the UWB, DWBPF predicts the possible region of the robot and randomly assigns particle samples in this region. The prediction and observation scores are substituted into the evaluation function, and the highest score region is obtained as the filter output. The contributions of the proposed system are listed as follows.

1) In the initial stage of robot motion, the odometer can provide high-precision tracking for the robot with a known starting orientation. Based on this property, the robot's position relative to the UWB anchor can be solved by triangulation and the least square method, which provides the initial coordinate input for DWBPF.
2) In the prediction stage of DWBPF, particles are randomly distributed in the dynamic window, rather than resampling the particles after the state transition [20], so it can solve the particle convergence problem of traditional PF well. In addition, a DWBPF resetting approach is proposed for the issues of robot lost track. When the deviation between the measurement radius and the dynamic window is greater than the error threshold, it is judged that the positioning system has lost the tracking of the robot, and DWBPF needs to be restarted.
3) The fusion algorithm can correct odometer error to reduce the odometer's cumulative error by using the odometer and UWB ranging measurement. Unlike existing UWB-based positioning systems, our approach requires only one anchor. The resulting system greatly reduces the required infrastructure and cost while providing long-term robot tracking with centimeter localization errors.

The remainder of the article is organized as follows. Section II summarizes related works in UWB-based positioning systems. The proposed DWBPF is described in Section III. In Section IV, experimental validation as well as discussions are presented and Section V concludes the article.

II. Related Works

In order to provide long-term and accurate tracking, the researchers used the global positioning technique to correct the local positioning, which was to fix the odometer's cumulative error through UWB. The UWB system obtains the distance between two nodes by calculating the time of flight (TOF). Two-way ranging (TWR) TOF enables measurement accuracy of 10 cm. Under ideal conditions, the maximum measurable range is 300 m [21].

For errors caused by NLOS, Suski et al. [22] proposed a method to establish a UWB measurement noise map, effectively reducing the impact of NLOS on positioning accuracy. But this method requires a significant amount of time to generate a measurement noise map. Zhu et al. [23] improved the error map method. Although their method reduces the number of measurement points by nearly 50%, it still needs a sufficient amount of prior knowledge and is not robust to dynamic environments.

Hybrid systems are the mainstream method to improve the accuracy of UWB-based positioning systems. Feng et al. [24] fused UWB and inertial measurement unit (IMU), Zhou et al. [25] fused UWB and radar, and Nguyen et al. [26] fused camera, IMU, and UWB. Although these hybrid positioning systems based on UWB can achieve centimeter accuracy and track targets robustly, they all need at least three anchors for position estimation. The UWB anchors need to be reasonably deployed, and the anchor coordinates must be used as prior knowledge of the positioning system. Therefore, they are not economical due to the costly infrastructure and difficult deployment.

Tian et al. [27] implemented a PF-based low-cost inertial navigation system (INS) and UWB fusion localization system, which can track the target with a known initial position using only one anchor. In order to mitigate the ranging errors caused by UWB, Tian et al. [28] proposed a novel adaptive UWB error mitigation scheme. It evaluates the uncertainty level based on the power quality metric of the UWB. Under NLOS conditions, only the Gamma distribution is used in the model. When the power metric cannot distinguish between the LOS and NLOS conditions, a combined Gaussian-Gamma distribution is used to characterize the error profile. The proposed model

is formulated in (1) where x, c_0, μ, σ represents the ranging measurement error, a constant term, mean, standard deviation (SD) of Gaussian distribution, λ, k denotes the parameters in Gamma distribution, Q represents the power metric for the UWB measurement

$$f(x) = \begin{cases} \frac{1}{\sigma\sqrt{2\pi}} \cdot e^{-\frac{(x-\mu)^2}{2\sigma^2}} \\ \quad \text{when } \overline{Q} < 6 \text{ dBm} \\ \frac{1}{\sigma\sqrt{2\pi}} \cdot e^{-\frac{(x-\mu)^2}{2\sigma^2}} + \lambda \cdot e^{-\lambda x} \cdot \frac{(\lambda x)^{k-1}}{\Gamma(k)} + c_0 \\ \quad \text{when } \overline{Q} \in [6, 10] \text{ dBm} \\ \lambda \cdot e^{-\lambda x} \cdot \frac{(\lambda x)^{k-1}}{\Gamma(k)} + c_0 \\ \quad \text{when } \overline{Q} > 10 \text{ dBm}. \end{cases} \tag{1}$$

When using sparse UWB anchors for positioning, the lost track issue may be encountered more frequently than with the conventional multianchor positioning system. Therefore, when the deviation of the particle cloud from the observed value is too large, that is, the lost track issue occurs, and the PF needs to be restarted. Turgut and Martin [29] proposed a model to make decisions based on measurements of the Kullback–Leibler divergence (KLD). If the KLD between the distribution implied by the observation and the distribution implied by the particle cloud is larger than a given threshold, the PF is restarted. Tian et al. [18] improved the particle restart method according to the UWB positioning model, changing the rectangular distribution into a circular distribution. However, the restart rule of this method is that it starts judging only when the tag approaches the anchor and then starts moving away, and the threshold parameter relies on engineering experience, thus having some limitations.

In the single anchor positioning system, the traditional PF has the problem of particle convergence and difficulty in establishing particle restart rules. In order to overcome these shortcomings, DWBPF is proposed in this article. The restart rule of this scheme does not need to satisfy specific trigger conditions. UWB power quality indicators also adaptively adjust the parameter weights to ensure that the dynamic window can represent the error well. The method achieves robust and accurate mobile robot tracking and is validated by actual tracking experiments.

III. Proposed Tracking Method

This section introduces the proposed DWBPF with an overview followed by descriptions of key components of the system.

A. Overview

The processing of the proposed system is shown in Fig. 1. The data update rates of the odometer and UWB are different, with the odometer having a higher update rate. Processing is triggered each time the UWB data is updated to ensure data synchronization. The odometer model in Section III-B gives a detailed description of this process. The localization system mainly consists of the Estimate initial position and long-term tracking of the mobile robot, which are described in detail in Sections III-C and III-D.

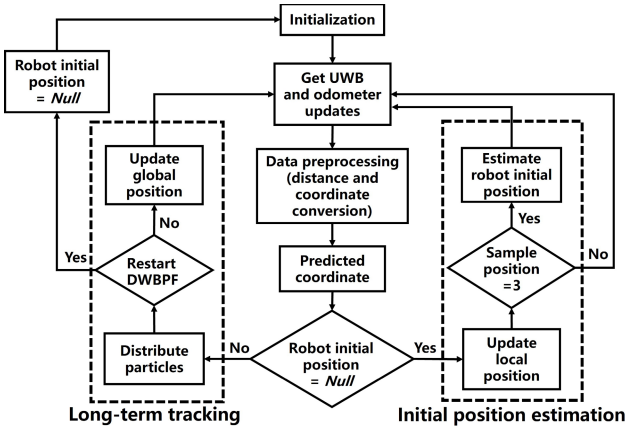

Fig. 1. Overview of the proposed system.

In the positioning system, the global coordinates of the anchor (x_a, y_a, z_a) are known because the anchor has been deployed in advance. The height h of the mobile robot is kept constant. The airline distance s measured by UWB can be converted into the horizontal distance d between the mobile robot and the anchor by the formula as follows:

$$d = \sqrt{s^2 - (z_a - h)^2}. \tag{2}$$

In the initialization stage of the positioning system, the mobile robot's head direction θ in the reference coordinate system must be known prior knowledge. Because in two coordinate systems with nonzero rotation angles (robot coordinate system and reference coordinate system), the initial position of the mobile robot cannot be estimated by only one anchor positioning system. The rotation matrix can align the robot coordinate system with the reference coordinate system so that the odometer update data is converted to the displacement distance in the reference coordinate system. Three appropriate sampling points can calculate the position of the anchor relative to the robot coordinate system and then the robot coordinate can be transformed to the reference coordinate system by coordinate translation, which completes the initial position estimation of the mobile robot. The filter fusion algorithm uses the same coordinate system in the long-term position tracking stage.

B. Differential Mobile Robot Motion Model

Mobile robots currently on the market or used in academic studies are commonly installed with photoelectric encoders. Therefore, we predict the robot's motion state by obtaining the odometer data through the encoder conversion to realize the prediction stage in the tracking filtering algorithm. The motion model is shown in Fig. 2. Δx and Δy are the displacement distance of the mobile robot in the x-axis and y-axis directions.

The forward distance of the driving wheel in the sampling time can be obtained by converting the data of the photoelectric encoder installed on the driving motor. Then Δx and Δy can be obtained by converting the forward distance of the driving wheel. Assuming that the diameters of the left and right driving wheels are d_L and d_R, the distance between the

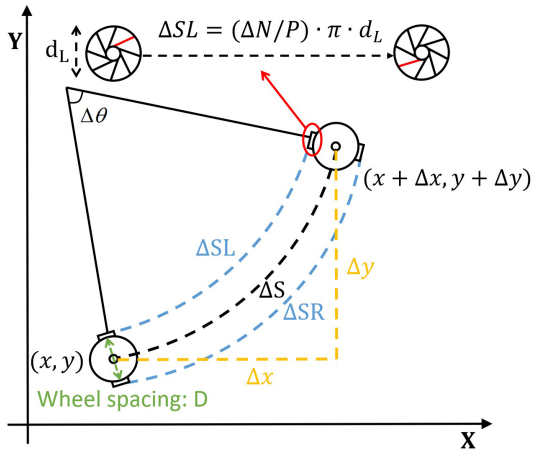

Fig. 2. Motion model.

left and right wheels of the mobile robot is D, the number of lines of the photoelectric encoder is P, and the increase in the number of pulses of the photoelectric encoder in Δt is ΔN. The forward distance of the mobile robot's left and right driving wheels is formulated in the following equation:

$$\begin{aligned} \Delta SL &= (\Delta N/P) \cdot \pi \cdot d_L \\ \Delta SR &= (\Delta N/P) \cdot \pi \cdot d_R. \end{aligned} \tag{3}$$

To obtain Δx and Δy in the robot coordinate system, we first converted the forward distance of the left and right drive wheels into the displacement distance ΔS and shifted angle $\Delta\theta$ of the robot, as formulated in the following equation:

$$\begin{aligned} \Delta S &= (\Delta SL + \Delta SR)/2 \\ \Delta\theta &= (\Delta SL - \Delta SR)/D. \end{aligned} \tag{4}$$

Δx and Δy can be converted through ΔS, $\Delta\theta$, and a known initial mobile robot's head direction θ, as formulated in the following equation:

$$\begin{aligned} \Delta x &= \Delta S \cdot [\sin(\theta + \Delta\theta) - \sin\theta]/\Delta\theta \\ \Delta y &= \Delta S \cdot [\cos\theta - \cos(\theta + \Delta\theta)]/\Delta\theta. \end{aligned} \tag{5}$$

The trajectory of the mobile robot can be obtained by accumulating the displacement distance of the mobile robot. In a short time, the motion model will be very close to the actual motion of the mobile robot. Because the forward distance of the left and right driving wheels obtained by the encoder is affected by the Moiré fringe photoelectric signal subdivision error, the trajectory has a cumulative error, which needs to be predicted and updated by filtering algorithm to eliminate the cumulative error.

C. Initial Position Estimation

The robot's initial position is estimated by applying trilateration in the estimated initial stage. And the least-square method is used to solve the optimal solution. We first select three sampling points and then record their robot coordinates (x_i, y_i) and the UWB horizontal distance d_i. Since the global coordinates of the anchor are known, the position of the anchor under the robot's coordinate system can be solved first and then the robot's position under the reference coordinate system can be solved by a coordinate transformation. Therefore, the estimated initial stage is carried out in the robot coordinate system. The equation to solve for the relative coordinates (x'_a, y'_a) of the anchor in the robot coordinate system is formulated in the following equation:

$$\left(x_i - x'_a\right)^2 + \left(y_i - y'_a\right)^2 = d_i^2, \quad i \in (1, 2, 3). \tag{6}$$

The selection of the three sampling points significantly impacts the accuracy of the initial position estimation. Due to the high short-term positioning accuracy and small cumulative error of the odometer, the error in the initial position estimation mainly comes from the ranging error of the UWB.

UWB ranging errors [28] mainly arise from inaccuracies in the obtained TOF due to the multipath effect when receiving data. In an open environment, the impact of multipath effects can be ignored. There will be a direct propagation path for data transmission in the air, and the first path component (FPC) will arrive at the receiver corresponding to the direct path at the earliest. The received signal power is likely more concentrated on FPC than other multipath components (MPCs). In the case of NLOS, the transmission power will be significantly attenuated as UWB waves pass through obstacles or disperse in more MPCs, resulting in more ambiguity when FPC determines the reception time stamp. In the case of LOS, UWB has a higher ranging accuracy.

Decawave [30] described the received signal power of the DW1000 Rx_Power and the signal power of the first path FP_Power. The difference between the two powers can quantify the quality of the UWB measurement. The metric, Q, is shown in formula (7) in the unit of dBm, where F_n is the amplitude value of the first path amplitude (point n) and C is the channel impulse response power value. We can determine whether the channel is LOS or NLOS according to the difference Q between these two powers. Empirically, if the difference Q is less than 6 dBm, the channel is more likely to be LOS, while if it is greater than 10 dBm, the channel is more likely to be NLOS

$$Q = 10 \times \log_{10}\left(\frac{C \times 2^{17}}{F_1^2 + F_2^2 + F_3^2}\right). \tag{7}$$

According to the ranging principle of UWB, three power differences can be obtained in one ranging cycle: $Q1$, $Q2$, and $Q3$. Since the ranging frequency of UWB is around 3.57 Hz, the channel characteristics are assumed to be stable during one ranging cycle. As the anchor can obtain two power differences $Q1$ and $Q3$, which are close in value, we define the power metric $\tilde{Q}$ of the UWB measurement as the average value of $Q1$ and $Q2$.

The measurement quality is quantified using the $\tilde{Q}$ value, and the three coordinate points are selected according to the value of $\tilde{Q}$, so that the error is guaranteed to be small. To ensure an optimal solution to formula (6), three coordinates that are not collinear need to be selected, that is, the robot's motion posture has changed. Due to sensor drift, we judge the angle between the coordinates to be 30°–150° as a significant change in attitude. According to the above sampling

Algorithm 1 Initial Position Estimation

Input:

(x_a, y_a), Anchor coordinates

(x'_t, y'_t), d'_t, $\widetilde{Q}_t$, Odometry coordinates, horizontal distance and power metric

Output:

while 1 **do**
  $t = t + 1$
  if $\widetilde{Q}_t < 6$ **then**
    // Record the first point
    if $(x_1, y_1) == Null$ **then**
      $(x_1, y_1) \leftarrow (x'_t, y'_t),\ d_1 \leftarrow d'_t$
      // Record the second point
    else if $(x_2, y_2) == Null$ **then**
      // The motion changes significantly
      if $\sqrt{(x_1 - x'_t)^2 + (y_1 - y'_t)^2} > 1$ **then**
        $(x_2, y_2) \leftarrow (x'_t, y'_t),\ d_2 \leftarrow d'_t$
      end if
      // Record the third point
    else if $(x_3, y_3) == Null$ **then**
      // The motion changes significantly
      if $\frac{\pi}{6} < |(arctan(\frac{y_2}{x_2}) - arctan(\frac{y'_t}{x'_t})| < \frac{5\pi}{6}$ **then**
        $(x_3, y_3) \leftarrow (x'_t, y'_t),\ d_3 \leftarrow d'_t$
      end if
    else if $(x_3, y_3) \neq Null$ **then**
      $(x'_a, y'_a) \leftarrow according(10)$
      break
    end if
  end if
end while

rules, three optimal coordinates are selected along with the corresponding distance values.

As there are two unknowns and three equations in (6), to solve for the relative coordinates of the anchor, the least-squares method is usually used to solve the contradictory equations. We convert formula (6) into a matrix as formulated in (8), where the values of A and B are formulated in the following equations:

$$A \begin{bmatrix} x'_a \\ y'_a \end{bmatrix} = B \tag{8}$$

$$A = \begin{bmatrix} x_1 - x_2 & y_1 - y_2 \\ x_1 - x_3 & y_1 - y_3 \\ x_2 - x_3 & y_2 - y_3 \end{bmatrix} B = \begin{bmatrix} \frac{d_2^2 - d_1^2 + x_1^2 - x_2^2 + y_1^2 - y_2^2}{2} \\ \frac{d_3^2 - d_1^2 + x_1^2 - x_3^2 + y_1^2 - y_3^2}{2} \\ \frac{d_3^2 - d_2^2 + x_2^2 - x_3^2 + y_2^2 - y_3^2}{2} \end{bmatrix}. \tag{9}$$

The optimal relative coordinates of the anchor are solved by formula (10). The overall robot initial position estimation pseudo-code is shown in Algorithm 1

$$\begin{bmatrix} x'_a \\ y'_a \end{bmatrix} = \left(A^T A\right)^{-1} A^T B. \tag{10}$$

After obtaining the position of the anchor under the robot coordinate system (x'_a, y'_a), the initial position of the robot can be obtained as $(x_a - x'_a, y_a - y'_a)$. The robot coordinates can be converted to the reference coordinate system by the coordinate translation matrix, as formulated in (11). $(\hat{x}_0, \hat{y}_0)$ is the initial input coordinate of DWBPF

$$\begin{bmatrix} \hat{x}_0 \\ \hat{y}_0 \\ 1 \end{bmatrix} = \begin{bmatrix} 1 & 0 & x_a - x'_a \\ 0 & 1 & y_a - y'_a \\ 0 & 0 & 1 \end{bmatrix} \begin{bmatrix} x_3 \\ y_3 \\ 1 \end{bmatrix} = \begin{bmatrix} x_3 + x_a - x'_a \\ y_3 + y_a - y'_a \\ 1 \end{bmatrix}. \tag{11}$$

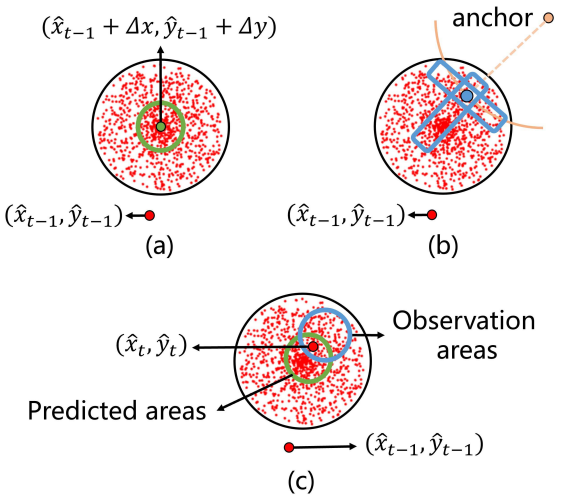

Fig. 3. DWBPF principle. Green is prediction areas, blue is observation areas, and red is optimal coordinates. (a) Predicted areas. (b) Observation areas. (c) Optimal coordinate solution.

D. Dynamic Window-Based Particle Filter

The traditional PF has the problem of particle convergence and difficulty in establishing particle restart rules. Our proposed improved particle filtering algorithm incorporates the ideas of DWA. The prediction stage is a random distribution of particles in a circular dynamic window, rather than resampling the particles after the transition, which solves the problem of particle convergence, as shown in Fig. 3. These particles predict the robot's position well because there is always a particle whose coordinates are close enough to the real coordinates of the robot.

The DWBPF uses particles in a dynamic window to represent the measurement error, so the radius r of the dynamic window is related to the mean and SD of the error model. From formula (1), it can be deduced that under LOS, the mean and SD are μ and σ, respectively, and under NLOS, the mean and SD are k/λ and $(k)^{1/2}/\lambda$. In LOS, the ranging error follows Gaussian distribution. According to the properties of Gaussian distribution, we believe that the ranging error has a 95% probability of appearing between $\mu - \sigma$ and $\mu + \sigma$. To ensure the robustness of the dynamic window, under NLOS, we consider that the errors are all larger than the mean k/λ, and the errors increase in proportion to the SD $(k)^{1/2}/\lambda$. After determining the LOS and NLOS's error range is between $\mu + \sigma$ and k/λ in the case that NLOS and LOS cannot be distinguished. Therefore, the measurement radius r is calculated as shown in the formula (12). For the lost track problem, we can convert this to the degree of deviation

of the measurement radius from the dynamic window. If the deviation reaches the lost track threshold, it is decided that the positioning system needs to restart the DWBPF

$$r = \begin{cases} (\mu-\sigma)+(2\cdot\sigma)\cdot\dfrac{\widetilde{Q}}{6}, & \widetilde{Q} < 6 \text{ dBm} \\ (\mu+\sigma)+\left(\dfrac{k}{\lambda}-(\mu+\sigma)\right)\cdot\dfrac{\widetilde{Q}-6}{10-6}, & \widetilde{Q}\in[6,10] \text{ dBm} \\ \dfrac{k}{\lambda}+\dfrac{\sqrt{k}}{\lambda}\cdot\left(\widetilde{Q}-10\right), & \widetilde{Q} > 10 \text{ dBm}. \end{cases} \tag{12}$$

After obtaining the possible region of the mobile robot, selecting an optimal coordinate as the filter output is necessary. Thus, we propose an evaluation function to evaluate the quality of each particle and calculate the corresponding score. In practice, systematic errors in the odometer can cause prediction errors, and multipath effects in the UWB can cause observation errors. Considering these errors, we divide the scores into two kinds of scores. One is the prediction score, that is, the closer the particle is to the predicted value, the higher the score. And the other is the observation score, that is, the closer the particle is to the observed value, the higher the score.

In the prediction score, we use the proximity of the particle to the predicted value as a measure, as shown in Fig. 3(a), that is, the distance between the calculated coordinates of each particle and the predicted coordinates, as formulated in (13). In the observation score, we divide it into an observation distance score and an observation angle score, as shown in Fig. 3(b). The distance score uses the proximity of the particle to the observation radius as a measure, that is, the distance from each particle to the measurement radius, as formulated in (14). The angle score uses the proximity of the particle to the observed angle as a measure, that is, the angular difference between the angle of each particle to the anchor and the angle of the predicted coordinates to the anchor, as formulated in (15). Finally, these metrics are inverted as the final score. The higher the proximity, the higher the score, and the maximum score is limited to 1000 to prevent an infinite score, as formulated in (16)

$$\text{pre}^{(i)} = \sqrt{\left(\left(\hat{x}_{t-1}+\Delta x\right)-z_x^{(i)}\right)^2+\left(\left(\hat{y}_{t-1}+\Delta y\right)-z_y^{(i)}\right)^2} \tag{13}$$

$$\text{dis}^{(i)} = \sqrt{\left(z_x^{(i)}-x_a\right)^2+\left(z_y^{(i)}-y_a\right)^2}-d \tag{14}$$

$$\text{deg}^{(i)} = \left|\arctan\left(\frac{z_y^{(i)}-y_a}{z_x^{(i)}-x_a}\right)-\arctan\left(\frac{\hat{y}_{t-1}+\Delta y-y_a}{\hat{x}_{t-1}+\Delta x-x_a}\right)\right| \tag{15}$$

$$\tilde{\omega}_P^{(i)} = \begin{cases} 1/P^{(i)}, & 0.001 < P^{(i)} \\ 1000, & P^{(i)} \le 0.001 \end{cases}, P\in(\text{pre},\text{dis},\text{deg}) \tag{16}$$

(z_x, z_y) is the coordinate of the particle, $(\hat{x}_{t-1}, \hat{y}_{t-1})$ is the output of the filter at the previous time, and (x_a, y_a) is the coordinate of the anchor.

In order to improve the robustness of DWBPF in complex environments, we propose an adaptive score matrix, as formulated in (17), where Z_{11} is the prediction weight, and Z_{12} is the observation weight. The larger $\tilde{Q}$ is, the larger the observation error will be, and DWBPF should trust the predicted value more. Therefore, the prediction weight is directly proportional to $\tilde{Q}$, while the observation weight is inversely proportional to $\tilde{Q}$. We take the maximum $\tilde{Q}$ value of 6 dBm under LOS as the dividing line. When $\tilde{Q}$ is less than 6 dBm, the observed weight is greater than the predicted weight, and when $\tilde{Q}$ is greater than 6 dBm, the predicted weight is greater than the observed weight

$$Z = \left[\tilde{Q}, 6^2/\tilde{Q}\right]. \tag{17}$$

After obtaining the sum of the scores of each particle, the particles were ranked according to their scores. The top 5% of the particles are selected as the optimal set of particles, and their average is used as the filter output coordinates, as shown in Fig. 3(c). The overall filtering pseudo-code is shown in Algorithm 2.

IV. Experimental Evaluation

The proposed DWBPF is implemented and evaluated with practical robot positioning experiments. Experimental setup and result analysis are presented in this section.

A. Devices and Experimental Setup

The mobile robot used in this experiment is the aimibot epidemic prevention robot (EPR). The body of EPR accommodates a balanced drive system (with four universal wheels and two direct drive wheels), reversible dc motor and drive electronic equipment, a high-resolution motion encoder, and battery power. It also has an ultrasonic, anti-drop sensor, a digital attitude sensor, and an NUC onboard computer.

In this experiment, we use the DW1000 UWB chip and STM32F1 minimum system as a node. The STM32 communicates with the DW1000 via the SPI protocol and controls the DW100 for data transmission and reception. After obtaining the corresponding timestamps, we calculate the difference in TOF and get the average TOF. Multiply it by the flight speed. We then get the distance. As the DW1000 has some systematic errors, the DW1000 needs to be externally calibrated using the method in [31] for both DW1000 chips. Finally, the distance data is brought into the calibration formula to obtain the exact distance between the two nodes.

The mobile node communicates with the EPR through RS232. The processing platform of the EPR reads the distance data and the power metric obtained from the tag. We publish the distance, power metric, and odometer data via a topic using the robot operating system (ROS). The terminal server in the same LAN subscribes to the topic published by the EPR through MATLAB, records all the data, and passes different filtering algorithms to verify the tracking performance of DWBPF.

This experiment has four parts: the UWB static-ranging error experiment, initial position estimation experiment, DWBPF tracking experiment, and DWBPF restart experiment.

Algorithm 2 DWBPF

Input:

x_a, y_a, Anchor coordinates
$\hat{x}_{t-1}, \hat{y}_{t-1}$, Previous time filtered output
$\Delta x, \Delta y$, Odometer increment
$d, \widetilde{Q}$, Horizontal distance and power metric

Output:

// Set the radius and center of the dynamic window
$r \leftarrow according(12)$
$o \leftarrow (\hat{x}_{t-1} + \Delta x, \hat{y}_{t-1} + \Delta y)$
// Determine whether to restart
$P_{ao} \leftarrow \sqrt{(o(1) - x_a)^2 + (o(2) - y_a)^2}$
// Restart if conditions are not met
if $|d - r| < P_{ao} < d + r$ **then**
  // Particles are distributed in the dynamic window
  for $i = 1 \rightarrow n$ **do**
    $r' \leftarrow rand() \cdot r$
    $\theta' \leftarrow rand() \cdot 2\pi$
    $z_x^{(i)} \leftarrow r' \cdot \cos\theta' + o(1)$
    $z_y^{(i)} \leftarrow r' \cdot \sin\theta' + o(2)$
  end for
  // Calculate score
  for $i = 1 \rightarrow n$ **do**
    $\tilde{\omega}_P^{(i)} \leftarrow according(16)$
  end for
  // Score normalization
  for $i = 1 \rightarrow n$ **do**
    $\omega_P^{(i)} \leftarrow \tilde{\omega}_P^{(i)} / \sum_{m=1}^{n} \tilde{\omega}_P^{(m)}$
  end for
  // Calculate the total score
  $Z \leftarrow according(16)$
  $\omega^{(i)} = \omega_{pre}^{(i)} \times Z_{11} + (\omega_{dis}^{(i)} + \omega_{deg}^{(i)}) \times Z_{12}$
  // Sort by ω
  $\tilde{\mu}^{(i)} = \left[\omega^{(i)}, z_x^{(i)}, z_y^{(i)}\right]$
  $\mu \leftarrow sort(\tilde{\mu})$
  // Save the coordinates of the first 5% of the score
  for $i = 1 \rightarrow n \cdot 5\%$ **do**
    $(x'^{(i)}, y'^{(i)}) \leftarrow (\mu_{i2}, \mu_{i3})$
  end for
  $(\hat{x}_t, \hat{y}_t) \leftarrow (mean(x'), mean(y'))$
end if

The experimental site is located in Laboratory 201, National Engineering Research Center for Robot Vision Perception and Control Technology, Hunan University. The layout of the experimental area is shown in Fig. 4. The experimental area is an open indoor environment, the reference path is a rectangle of 3 × 2 m, and the lap distance is 10 m. To verify the effectiveness and robustness of DWBPF, we placed a rectangular obstacle with a side length of 0.3 m within the range of the reference path to make the EPR appear NLOS during movement. The anchor node is arranged at a height of 2 m, and the coordinate of the anchor is defined as the origin of the coordinate system. The x-axis is parallel to the wall where the anchor is installed. We mark eight sampling points on the floor to evaluate the tracking accuracy: the four vertices

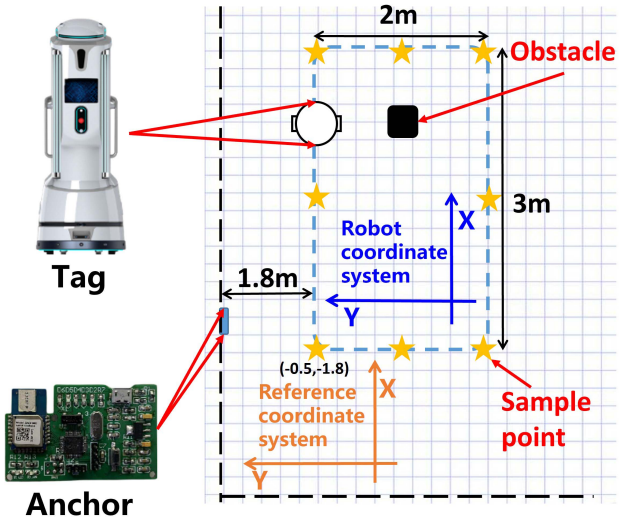

Fig. 4. Experimental area.

TABLE I
PROPOSED DWBPF PARAMETER SETTINGS

Parameter	Value
μ(m)	0.1
σ(m)	0.055
λ	3.5
k	2

of the reference path and the midpoints of the four edges. The starting point of the EPR is set as $(-0.5, -1.8)$. When the EPR passes through a sampling point, the laser rangefinder is used to obtain the coordinates of the EPR, and the odometer coordinates and filtered output coordinates are recorded.

The starting and ending positions of the localization experiment were the sample points closest to the anchor. In the tracking experiment, the EPR repeated the reference path seven times for a total trip of 70 m and obtained 56 groups of sample point data. In the restart experiment, we make the wheel of the EPR slip between the fifth and sixth sample points, resulting in the continuous increase of the EPR odometer data, but the actual position does not change, which will lead to a serious lost track problem. After the EPR skidded, the reference path was repeated three times to obtain 24 groups of sampling point data. In addition to the obstacle objects we arranged, no other NLOS obstacles, such as people and walls, were introduced in the experiment. The parameter settings in the proposed DWBPF are summarized in Table I. The parameter settings of the UWB distance measurement error model use the same values as provided in [21]. The Gaussian distribution has a mean value of 0.1, and SD equals 0.055. The Gamma distribution is defined by parameters λ and k equal to 3.5 and 2, respectively.

B. Results and Discussions

First, we test the ranging effect of UWB in an open environment. The test distance is 2 ∼ 10 m and the distance

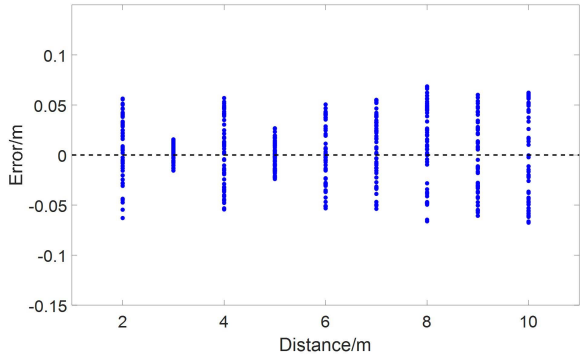

Fig. 5. Static error.

TABLE II
INITIAL POSITION ESTIMATION

	First Track	Second Track	Third Track
Robot initial position (m)	(1.5, -1.8)	(1, -0.5)	(0.5, -3)
Initial position esmation (m)	(1.47, -1.48)	(1.11, -0.47)	(0.52, -2.91)
Robot initial position error (m)	0.32	0.11	0.09

interval is 1 m. We measure 50 sets of distance data at each test point and calculate the differences from the real distance data as the errors, as shown in Fig. 5. Due to the introduction of the calibration equation, the measured value fluctuates up and down around the real value, with the maximum error of 0.082 m and an average error of 0.026 m.

To verify the effect of initial position estimation, we let the EPR move randomly from different initial positions in the experimental field. After the EPR obtains three sampling points that meet the conditions in (6), the initial coordinates are solved, and the results are shown in Table II. The average error of the estimated coordinates of the initial position is 0.17 m.

When the EPR's initial position is obtained, the EPR is controlled to move to the start point of the experiment, and the tracking experiment is carried out. The results of the tracking experiment are shown in Fig. 6. Fig. 6(a) shows the trajectory estimated by the odometer, Fig. 6(b) shows the trajectory estimated by the traditional PF, Fig. 6(c) shows the trajectory estimated by the proposed DWBPF, and Fig. 6(d) shows the error of the three estimated trajectories at the sample point. In the trajectory of the odometer, the odometer is affected by the cumulative error, which leads to the position shift of the odometer, and the error increases significantly in the latter stage of the movement. The trajectory of the traditional PF does not drift significantly, but there is a tilt in the lower right part of the motion path, which is the error caused by NLOS, but with the EPR's movement, this error caused by NLOS is eliminated. The trajectory of the proposed DWBPF is closer to the ground truth trajectory, and no obvious tilted occurs in the NLOS road segment. The error curves show the long-term reliability of the proposed DWBPF as well as its robustness in complex environments.

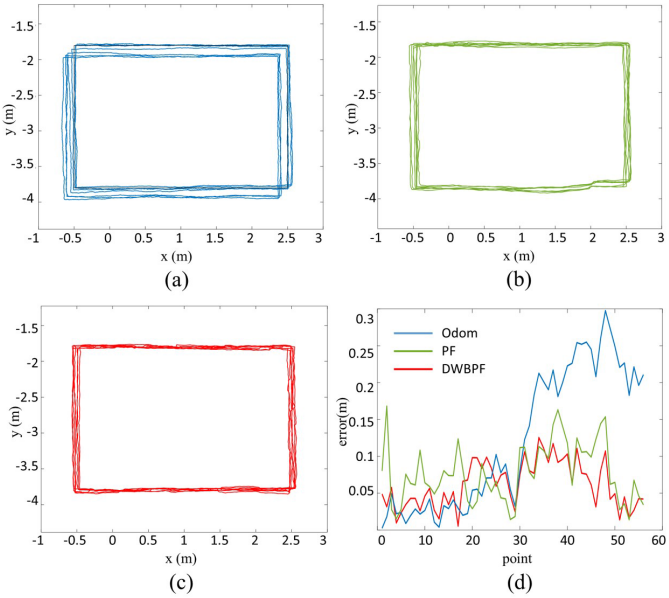

Fig. 6. Tracking paths of the experiment. (a) Odometer. (b) PF. (c) DWBPF. (d) Positioning error.

TABLE III
QUANTIZED TRACKING PERFORMANCE

	Odom	PF	DWBPF
point 1	(-0.58, -1.89)	(-0.49, -1.84)	(-0.52, -1.81)
point 2	(0.90, -1.88)	(0.92, -1.83)	(0.92, -1.82)
point 3	(2.39, -1.88)	(2.45, -1.83)	(2.43, -1.83)
point 4	(2.42, -2.86)	(2.47, -2.80)	(2.45, -2.81)
point 5	(2.42, -3.85)	(2.48, -3.79)	(2.46, -3.81)
point 6	(0.93, -3.87)	(1.00, -3.88)	(0.97, -3.83)
point 7	(-0.57, -3.89)	(-0.50, -3.86)	(-0.54, -3.83)
point 8	(-0.60, -2.91)	(-0.52, -2.86)	(-0.55, -2.84)

The quantized tracking performance results are shown in Table III. We analyzed the 56 groups of sampled data to find the average and maximum errors, respectively. The maximum errors of the three estimation methods are 0.298, 0.189, and 0.125 m, respectively, and the average errors are 0.132, 0.086, and 0.061 m, respectively.

In the restart experiment, we first repeated the above experiment. When the EPR passes the fifth sample point, we idle the EPR's wheels to simulate the robot slipping phenomenon. When the displacement increment of the odometer reaches 2 m, we let the EPR move normally, and then the robot has already suffered a serious lost track problem, as shown in Fig. 7(a). The black curve is the reference trajectory, and the blue curve is the trajectory estimated by the odometer. After the EPR resumed motion, we let the EPR repeat the reference trajectory twice, and the trajectory estimated by DWBPF is shown in Fig. 7(b). The blue marks are the coordinates where DWBPF recognizes the out-of-track phenomenon, and the green marks are the coordinates after DWBPF restarts.

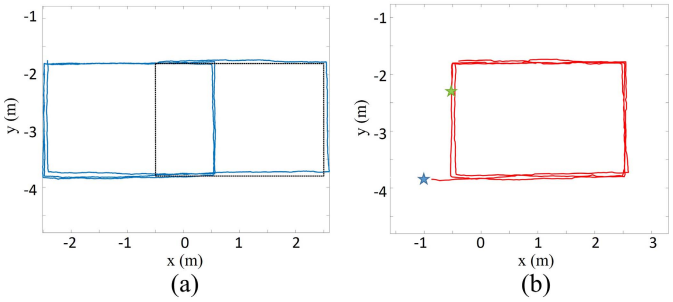

Fig. 7. DWBPF restart experiment. (a) Odometer. (b) DWBPF.

The coordinate error after restart is 0.13 m, which is the same as the second experiment's initial position estimation coordinate error. The tracking error of subsequent DWBPF is consistent with that of the third experiment.

The DWBPF proposed in this article aims to reduce the cost of the positioning system and enhance the tracking performance of the positioning system. The experimental results show that DWBPF still has good tracking performance in the NLOS environment, and the restart method of DWBPF can ensure the system's long-term performance. DWBPF solves the problem of skid and kidnapping of robots well and has accurate and long-term performance in robot positioning.

V. Conclusion

Compared with the traditional UWB indoor positioning scheme, the positioning system based on the odometer and UWB fusion proposed in this article has a lower cost, and only one anchor can be used to achieve global positioning. Instead of the error model, DWBPF uses randomly distributed particles, that is, a dynamic window is used to represent the observation and prediction errors. The range of the dynamic window is adaptively adjusted according to the received signal power quality metric, and the score weight is adaptively adjusted according to the metric, which still has accurate and stable robust performance in complex environments. The restart scheme of DWBPF does not rely on an exact error model and does not need to satisfy specific triggering conditions. Only the window size and the measurement radius are used to determine whether the restart condition is met. Experiments show that DWBPF can achieve centimeter-level positioning, and the average positioning error is 0.061 m, which realizes long-term and accurate mobile robot tracking.

The accuracy of the proposed DWBPF algorithm will be affected by the initial position prediction and UWB ranging accuracy. The localization effect of this algorithm is not good in a large-scale and multiscene indoor environment. Therefore, our future work focuses on improving the accuracy of the initial coordinates of the robot and adding additional anchors to increase the positioning range.

References

[1] S. Khan and J. Daudpoto, "Development of low-cost autonomous robot," in *Proc. Innov. Intell. Syst. Appl. Conf. (ASYU)*, 2019, pp. 1–6.

[2] J. Bai, J. Cai, T. Zhou, J. Li, S. Gao, and J. Bai, "Research on key technologies of meal delivery robot based on the fusion of lidar and machine vision," in *Proc. 7th Int. Conf. Big Data Inf. Anal. (BigDIA)*, 2021, pp. 236–242.

[3] X. Zhou, W. Wang, T. Wang, Y. Lei, and F. Zhong, "Bayesian reinforcement learning for multi-robot decentralized patrolling in uncertain environments," *IEEE Trans. Veh. Technol.*, vol. 68, no. 12, pp. 11691–11703, Dec. 2019.

[4] H. Zhang, W. Hong, and M. Chen, "A path planning strategy for intelligent sweeping robots," in *Proc. IEEE Int. Conf. Mechatronics Autom. (ICMA)*, Aug. 2019, pp. 11–15.

[5] "Overview of global positioning systems," in *Handbook of Position Location: Theory, Practice, and Advances*. IEEE, 2019, pp. 655–705.

[6] J. Li, L. Cheng, H. Wu, L. Xiong, and D. Wang, "An overview of the simultaneous localization and mapping on mobile robot," in *Proc. Int. Conf. Modeling, Identificat. Control*, 2012, pp. 358–364.

[7] L. Zhang, R. Zapata, and P. Lepinay, "Self-adaptive Monte Carlo localization for mobile robots using range sensors," in *Proc. IEEE/RSJ Int. Conf. Intell. Robots Syst.*, Oct. 2009, pp. 1541–1546.

[8] L. Batistić and M. Tomic, "Overview of indoor positioning system technologies," in *Proc. 41st Int. Conv. Inf. Commun. Technol., Electron. Microelectron. (MIPRO)*, May 2018, pp. 0473–0478.

[9] S. A. S. Mohamed, M.-H. Haghbayan, T. Westerlund, J. Heikkonen, H. Tenhunen, and J. Plosila, "A survey on odometry for autonomous navigation systems," *IEEE Access*, vol. 7, pp. 97466–97486, 2019.

[10] A. Jha and M. Kumar, "Two wheels differential type odometry for mobile robots," in *Proc. 3rd Int. Conf. Rel., Infocom Technol. Optim.*, Oct. 2014, pp. 1–5.

[11] X. Gao, S. Li, and Q. Ma, "Subdivided error correction method for photoelectric axis angular displacement encoder based on particle swarm optimization," *IEEE Trans. Instrum. Meas.*, vol. 69, no. 10, pp. 8372–8382, Oct. 2020.

[12] A. R. Jimenez and F. Seco, "Comparing decawave and bespoon UWB location systems: Indoor/outdoor performance analysis," in *Proc. Int. Conf. Indoor Positioning Indoor Navigat. (IPIN)*, Oct. 2016, pp. 1–8.

[13] S. Venkatesh and R. M. Buehrer, "Non-line-of-sight identification in ultra-wideband systems based on received signal statistics," *IET Microw., Antennas Propag.*, vol. 1, no. 6, pp. 1120–1130, 2007.

[14] J. Zhang, J. Salmi, and E.-S. Lohan, "Analysis of kurtosis-based LOS/NLOS identification using indoor MIMO channel measurement," *IEEE Trans. Veh. Technol.*, vol. 62, no. 6, pp. 2871–2874, Jul. 2013.

[15] S. Venkatesh and R. M. Buehrer, "NLOS mitigation using linear programming in ultrawideband location-aware networks," *IEEE Trans. Veh. Technol.*, vol. 56, no. 5, pp. 3182–3198, Sep. 2007.

[16] J. Riba and A. Urruela, "A non-line-of-sight mitigation technique based on ML-detection," in *Proc. IEEE Int. Conf. Acoust., Speech, Signal Process. (ICASSP)*, May 2004, p. 153.

[17] Z. Li, W. Trappe, Y. Zhang, and B. Nath, "Robust statistical methods for securing wireless localization in sensor networks," in *Proc. 4th Int. Symp. Inf. Process. Sensor Netw. (IPSN)*, Apr. 2005, pp. 91–98.

[18] Q. Tian, K. I. Wang, and Z. Salcic, "A resetting approach for INS and UWB sensor fusion using particle filter for pedestrian tracking," *IEEE Trans. Instrum. Meas.*, vol. 69, no. 8, pp. 5914–5921, Aug. 2020.

[19] M. Seder and I. Petrovic, "Dynamic window based approach to mobile robot motion control in the presence of moving obstacles," in *Proc. IEEE Int. Conf. Robot. Autom.*, Apr. 2007, pp. 1986–1991.

[20] C. Stachniss and W. Burgard, *Particle Filters for Robot Navigation*. America: Now Foundations and Trends, 2014.

[21] A. R. J. Ruiz and F. S. Granja, "Comparing ubisense, bespoon, and decawave UWB location systems: Indoor performance analysis," *IEEE Trans. Instrum. Meas.*, vol. 66, no. 8, pp. 2106–2117, Aug. 2017.

[22] W. Suski, S. Banerjee, and A. Hoover, "Using a map of measurement noise to improve UWB indoor position tracking," *IEEE Trans. Instrum. Meas.*, vol. 62, no. 8, pp. 2228–2236, Aug. 2013.

[23] X. Zhu, J. Yi, J. Cheng, and L. He, "Adapted error map based mobile robot UWB indoor positioning," *IEEE Trans. Instrum. Meas.*, vol. 69, no. 9, pp. 6336–6350, Sep. 2020.

[24] D. Feng, C. Wang, C. He, Y. Zhuang, and X.-G. Xia, "Kalman-Filter-Based integration of IMU and UWB for high-accuracy indoor positioning and navigation," *IEEE Internet Things J.*, vol. 7, no. 4, pp. 3133–3146, Apr. 2020.

[25] H. Zhou, Z. Yao, and M. Lu, "UWB/LiDAR coordinate matching method with anti-degeneration capability," *IEEE Sensors J.*, vol. 21, no. 3, pp. 3344–3352, Feb. 2021.

[26] T. H. Nguyen, T.-M. Nguyen, and L. Xie, "Range-focused fusion of camera-IMU-UWB for accurate and drift-reduced localization," *IEEE Robot. Autom. Lett.*, vol. 6, no. 2, pp. 1678–1685, Apr. 2021.

[27] Q. Tian, K. I.-K. Wang, and Z. Salcic, "A low-cost INS and UWB fusion pedestrian tracking system," *IEEE Sensors J.*, vol. 19, no. 10, pp. 3733–3740, May 2019.

[28] Q. Tian, K. I.-K. Wang, and Z. Salcic, "An INS and UWB fusion approach with adaptive ranging error mitigation for pedestrian tracking," *IEEE Sensors J.*, vol. 20, no. 8, pp. 4372–4381, Apr. 2020.
[29] B. Turgut and R. P. Martin, "Restarting particle filters: An approach to improve the performance of dynamic indoor localization," in *Proc. IEEE Global Telecommun. Conf. (GLOBECOM)*, Nov. 2009, pp. 1–7.
[30] Decawave. *DW1000 User manual*. Accessed: Dec. 17, 2018. [Online]. Available: https://www.decawave.com/sites/default/files/resources/dw1000_user_manual_2.11.pdf
[31] X. Zhou, H. Zhang, X. Tan, and J. Zhang, "A location method based on UWB for ward scene application," in *Proc. 36th Youth Academic Annu. Conf. Chin. Assoc. Automat. (YAC)*, 2021, pp. 66–71.

Hui Zhang (Member, IEEE) received the B.S., M.S., and Ph.D. degrees in pattern recognition and intelligent system from Hunan University, Changsha, China, in 2004, 2007, and 2012, respectively.

He is currently a Professor with the School of Robotics, Hunan University, and the Deputy Director of the National Engineering Laboratory for Robotic Vision Perception and Control Technology. His research interests include machine vision, image processing, and visual tracking.

Xidong Zhou (Graduate Student Member, IEEE) received the B.S. degree from the University of South China, Hengyang, China, in 2020. He is currently pursuing the M.Sc. degree with the School of Electrical and Information Engineering, Changsha University of Science and Technology, Changsha, China.

His current research interests include path planning of mobile robots, localization, and mapping.

Hang Zhong (Member, IEEE) received the B.S., M.S., and Ph.D. degrees in automation from the College of Electrical and Information Engineering, Hunan University, Changsha, China, in 2013, 2016, and 2020 respectively.

He is currently a Postdoctoral Researcher at the National Engineering Laboratory of Robot Visual Perception and Control Technology, Hunan University. His current research interests include robotics modeling and control, visual servo control, and path planning of aerial robots.

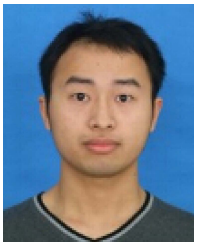

He Xie received the B.S. degree in mechanical design, manufacturing and automation, and the Ph.D. degree in mechatronic engineering from the Huazhong University of Science and Technology (HUST), Wuhan, China, in 2013 and 2019, respectively.

He has been a Postdoctoral Researcher with Hunan University, Changsha, China. His research interests include robot vision and manufacturing automation.

Wei He received the B.Eng. degree in automation and the M.Eng. degree in control science and engineering from the College of Automation Science and Engineering, South China University of Technology, Guangzhou, China, in 2006 and 2008, respectively, and the Ph.D. degree in control science and engineering from the Department of Electrical and Computer Engineering, National University of Singapore, Singapore, in 2011.

His current research interests include robotics, distributed parameter systems, and intelligent control systems.

Xuan Tan received the B.S. degree from the Changsha University of Science and Technology, Changsha, China, in 2020, where he is currently pursuing the M.Sc. degree with the School of Electrical and Information Engineering.

His research interest is focused on robot navigation, perception and localization, and lidar mapping.

Yaonan Wang received the Ph.D. degree in electrical engineering from Hunan University, Changsha, China, in 1994.

He was a Postdoctoral Research Fellow with the Normal University of Defense Technology, Changsha, from 1994 to 1995. From 1998 to 2000, he was a Senior Humboldt Fellow in Germany. From 2001 to 2004, he was a Visiting Professor at the University of Bremen, Bremen, Germany. From 2001 to 2020, he was the Dean of the College of Electrical and Information Engineering, Hunan University, where he has been a Professor since 1995. He is a Principle Leader at the National Engineering Laboratory of Robot Visual Perception and Control Technology, Hunan, China. His current research interests include intelligent control, robotics, and image processing. Dr. Wang is the Chairperson of the China Society of Image and Graphics, Beijing, China. He is a Fellow of the Chinese Academy of Engineering.